Collapses of two-dimensional granular columns

Gert Lube,[1] Herbert E. Huppert,[2] R. Stephen J. Sparks,[3] and Armin Freundt[1]
[1]*Research Division "Dynamics of the Ocean Floor," IFM-GEOMAR, Leibniz Institute for Marine Sciences, Wischhofstrasse 1-3, D-24148 Kiel, Germany*
[2]*Institute of Theoretical Geophysics, Department of Applied Mathematics and Theoretical Physics, Centre of Mathematical Sciences, University of Cambridge, Wilberforce Road, Cambridge CB3 0WA, United Kingdom*
[3]*Centre of Environmental and Geophysical Flows, Department of Earth Sciences, Bristol University, Bristol BS8 1RJ, United Kingdom*
(Received 23 December 2004; revised manuscript received 11 July 2005; published 4 October 2005)

The first detailed quantitative observations of the two-dimensional collapse of a granular column along a horizontal channel are presented for a variety of materials. Together with the complementary study for the axisymmetric situation, we conclude that for granular collapses the generally accepted approaches, that are highly dependent on frictional parameters, do not describe the main flow phenomena. The motion divides in two main flow regimes at $a \sim 1.8$, where the aspect ratio $a = h_i/d_i$ and h_i and d_i are the initial height and width of the column. We describe the details of collapse by emphasizing the sequential occurrence of a main spreading followed by a final avalanching phase. For the low a regime, $a < 1.8$, we derive descriptions of the final geometry by direct physical arguments. For the large a regime, $a > 1.8$, we determine that nearly all details of the collapse, including the position of the flow front as a function of time, the emplacement time, the self-similar final profiles, and especially their maximum vertical and horizontal extension, are established during the spreading phase and can be expressed in terms of the initial geometrical parameters but are independent of basal and internal friction parameters.

DOI: 10.1103/PhysRevE.72.041301 PACS number(s): 45.70.Mg, 83.80.Fg

I. INTRODUCTION

The flow of granular media plays an important role in many different areas, including agriculture, chemical engineering, the Earth Sciences, fundamental physics, hazard management, and the pharmaceutical industry. Partly because of this multidisciplinary nature there has been considerable research interest in this area recently. In differing circumstances a granular medium can behave like a solid, a liquid, or a gas. Three inspiring reviews use these analogies as the foundation [1–3] and have discussed the change from one form to another, somewhat akin to a phase transition. However, the major obstacle in all this work and the aim of many recent studies has been the absence of general governing equations to describe the motion and behavior of granular media. This is in marked contrast to the understanding of solids, liquids, and gases, where the equations of statics have been known for centuries and the theory of linear elasticity, the Navier-Stokes equations, and the kinetic theory of gases have almost a century of investigation.

Some progress has been made to develop an understanding of granular media. For flowing granular media, equations akin to the shallow water equations of fluid mechanics [4,5] have been developed for a monodispersed granular medium flowing in steady state down an inclined plane at an angle to the horizontal greater than the static angle of repose [6–10 and references therein]. These equations emphasize frictional effects between the grains and along the bottom boundary, and also assume that variations in the slope of the free surface are small. It is not yet clear how well these equations will apply to large-scale flows, as are commonly observed in the gigantic rockfalls which occur on the Earth, the Moon, and Mars, involving up to 10^4 km^3, in contrast to the 10^3 cm^3 in laboratory experiments [11–16]. As in many areas of science, experimental data help to develop the intuition needed for the derivation of the fundamental equations; and indeed many experiments with granular flows have been conducted. However, one difficulty is that, unlike other fluid-mechanical systems, sometimes the flow behavior can depend on the distance between bounding walls, even when the distance is much larger than the size of the granular material itself [17,18].

Recently, we initiated a fundamental experimental investigation on the collapse of an initially cylindrical volume of granular material released instantaneously onto a rough horizontal bed [19]. Unknown to the present authors, a similar study was undertaken by a French group [20]. These axisymmetric studies show that the major governing parameter is the aspect ratio a, defined as the ratio of the initial height, h_i, to the initial radius, r_i, of the cylinder of granular material. Almost all of the details of the collapse, such as the time, t_∞, taken to reach the final runout distance, r_∞, and the final height at the center of the resultant deposit, h_∞, were found to be independent of the different grains used—couscous, rice, salt, sand, and sugar—and the roughness of the lower boundary. Basal frictional effects are minimal because a thin layer of particles is lain down over which the main flow rides. Intergranular frictional effects are dominated by inertial forces, until very near the end of the collapse, where the flows come to a quite abrupt halt (except for some thin, small scale avalanching which occurs on the upper free surface of the deposit).

The aim of the present paper is to investigate the details of the collapse in a two-dimensional geometry. The paper is not just a presentation of results in a different geometry, but builds on and extends the intuition and techniques developed for the axisymmetric investigation utilizing the advantage to observe the flows in cross section. The plan of the paper is as

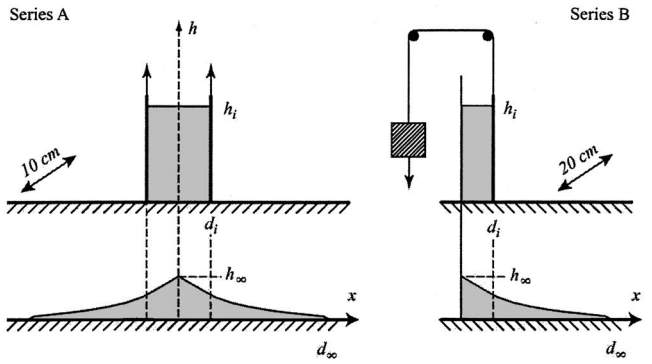

FIG. 1. Initial setups for the experiments of series A and B with a rough sketch of the final deposit beneath.

follows. We explain the two experimental setups and techniques in Sec. II and describe the observations in Sec. III. Section IV presents quantitative representations of the shape of the final deposit, including the final runout distance and maximum central height, and the time for collapse, which are represented by simple power-law functions of the initial aspect ratio. A collapse of all the data for the nondimensional position of the front as a function of nondimensional time is also documented. The final section summarizes our study, compares the results with the previous axisymmetric studies, and draws some conclusions. The two-dimensional results presented here were first announced in the conference proceedings [21].

II. THE EXPERIMENTS

A. Experimental setups

The experiments investigate two-dimensional granular flows created by rapidly releasing particulate columns, initially contained in a rectangular box, into a wide channel. Two main experimental series were studied using different setups.

Series A involved symmetric spreading along a channel that had a constant width of 10 cm [Fig. 1(a)]. The rear panel and the base of the tank, constructed of wood, were covered with a thin sheet of paper, whereas the front panel was transparent Plexiglas. Lube *et al.* [19] showed that the roughness of the floor made no difference to the results, because, irrespective of the roughness of the surface, a thin layer of grains was deposited and the main flow took place over these stationary grains. Moreover, the general validity of this result

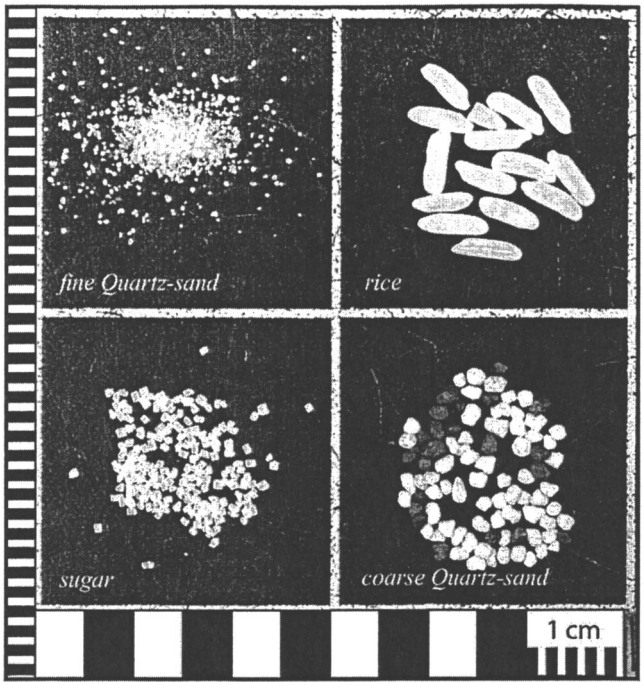

FIG. 2. Photo of the four different types of grain used in the experiments with millimeter markings on the side and half centimeter markings at the bottom.

was confirmed here by some additional experiments performed using a rough surface made of sandpaper with roughness of the same order as the flowing sand. The container in which the initial columns were prepared consisted of two parallel, vertically movable gates. Symmetrical column collapses resulted from the fast manual lifting of the gates [Fig. 1(a)]. The geometry of the initial columns was varied by using different horizontal spacing of the gates and different masses of material. We carried out experiments with two different quartz sands, rice, and sugar, thus covering a wide range of grain sizes and shapes. Grain sizes were chosen so that cohesion effects would be negligible. A photo of the different sets of grains, clearly showing their different geometrical shapes, is given in Fig. 2. Density, mean grain size, and angle of repose for each set of material are given in Table I.

Experiments of series B involved unidirectional spreading and were performed in a tank of 20 cm width. A different type of container to accommodate the initial particulate columns was connected to one end of the tank. The rectangular box of the same width as the channel and variable initial

TABLE I. Properties of particles used in the experiments.

Particle	Mean density (g/cm^3)	Mean grain size (mm)	Angle of repose (deg.)
Fine quartz sand	2.6	0.15	29.5
Coarse quartz sand	2.6	1.5	31
Sugar	1.58	1	35
Rice	1.46	7×2[a]	32

[a]Long axis × short axis.

TABLE II. Initial basal length and range of aspect ratio for each material.

Experiment	Particle	Initial basal length (cm)	Range of $a=h_i/d_i$
Series A	Fine quartz sand	1.95	0.7–7.6
	Coarse quartz sand	1.95	0.5–17
		4.8	0.6–8.6
	Sugar	1.95	1–21
	Rice	1.95	1–18
Series B	Coarse quartz sand	4.5	0.7–18
		8.3	0.5–11
		12.5	2–4.7

basal length d_i comprised only one frontal gate to release the granular material [Fig. 1(b)]. A release mechanism was constructed to allow for very fast and reproducible lifting velocities of the gate. It consisted of releasing a large weight connected to the gate via a pulley construction at the ceiling. The weight fell free for the first 0.75 m to reach a high velocity before it lifted the gate nearly instantaneously. The time for the gate release in any experiment was very much less than the typical time scale of the resulting motion.

In both series the initial aspect ratio a, defined by the ratio of initial height, h_i, to initial basal distance, d_i, was varied systematically over two orders of magnitude. The initial basal lengths and range of aspect ratios for each set of grains and experimental series are presented in Table II.

B. Measurement methods

Both sets of experiments were recorded by video to investigate the behavior of the collapses through the vertical Plexiglas plane. A normal 25 frames per second (fps) camera was used for series A, whereas a fast industrial camera at 240 fps was employed in series B. Data for distance against time of the flow front were obtained from the movie sequences by measuring the elapsed time at horizontal markings in spacings of 3 mm. We used three different approaches to study flow and sedimentation processes in detail. In order to measure the geometry and the continuously reducing volume of the flowing layer as a function of time, we mapped the free surface and the interface between deposited and static material by manually cross-correlating between neighboring frames of a high-speed sequence. For some experiments, we also observed the deformation of the flowing layer by calculating the intensity difference between consecutive images. Velocity profiles with depth in the flowing layer were obtained using the particle image velocimetry (PIV) algorithm written by Dalziel [22].

After each run, the contour of the final deposit was measured to determine d_∞, the maximum runout distance and h_∞, the maximum deposit height at $x=0$. The measuring system consisted of the combination of a grid printed on the vertical transparent plane and a point laser projected horizontally at variable heights onto the pile. The accuracy in determining the granular surface height is limited by grain size. However, the optical resolution was higher than the mean grain size of all tested grains except for fine quartz sand.

III. EXPERIMENTAL OBSERVATIONS

Qualitative observations of granular collapses within a channel reveal a strong dependence of the flow behavior on the value of the initial aspect ratio a, as found for axisymmetric collapses by Lube *et al.* [19] and Lajeunesse *et al.* [20]. To help emphasize the similarities and differences between the two-dimensional and axisymmetric collapses, we will first explain the two major flow regimes in the quasi-two-dimensional situation and the general modes of granular flow observed. We then give a detailed description of the internal deformation and sedimentational processes as seen in the high-speed movies filmed through the Plexiglas plane.

A. Flow regimes and form of final deposits

In Fig. 3 we depict images from experiments with aspect ratios of 0.5, 1.5, and 7 to illustrate the two flow regimes, namely that of *low* [Figs. 3(a)–3(h)] and *high* aspect ratios [Figs. 3(i)–3(l)], and two modes of granular flow behavior which are found to determine the shape of the final deposits. The most apparent difference between the two regimes is that for low values of a only the edges of the initial column are in motion [Figs. 3(a) and 3(e)], whereas for large a the entire free surface flows from the beginning [Fig. 3(i)]. In a similar manner to axisymmetric collapses, the different behavior dependent on a stems from the development of an initial failure plane along which material flows down, and below which particles remain static [Figs. 3(a), 3(e), and 3(i)].

The geometrical position of this initial discontinuity, which has a conical geometry in the axisymmetric case, was observed in two ways. In cross-sectional view through the Plexiglas plane the discontinuity has the same initial position independent of the value of the aspect ratio and the grain type. It appears as a straight line intercepting at a zero height at $x=d_i$, where x is the distance from the origin, which is inclined at 61° to the horizontal. For experiments with aspect ratios less than 1.8, the discontinuity can also be initially observed as a straight line on the upper free surface of the column [Fig. 3(a)]. We measured the horizontal distance, d_a, between that line and $x=0$ for several experiments. When normalized by d_i and plotted against the aspect ratio (Fig. 4) the data are accurately represented by the best-fit linear form

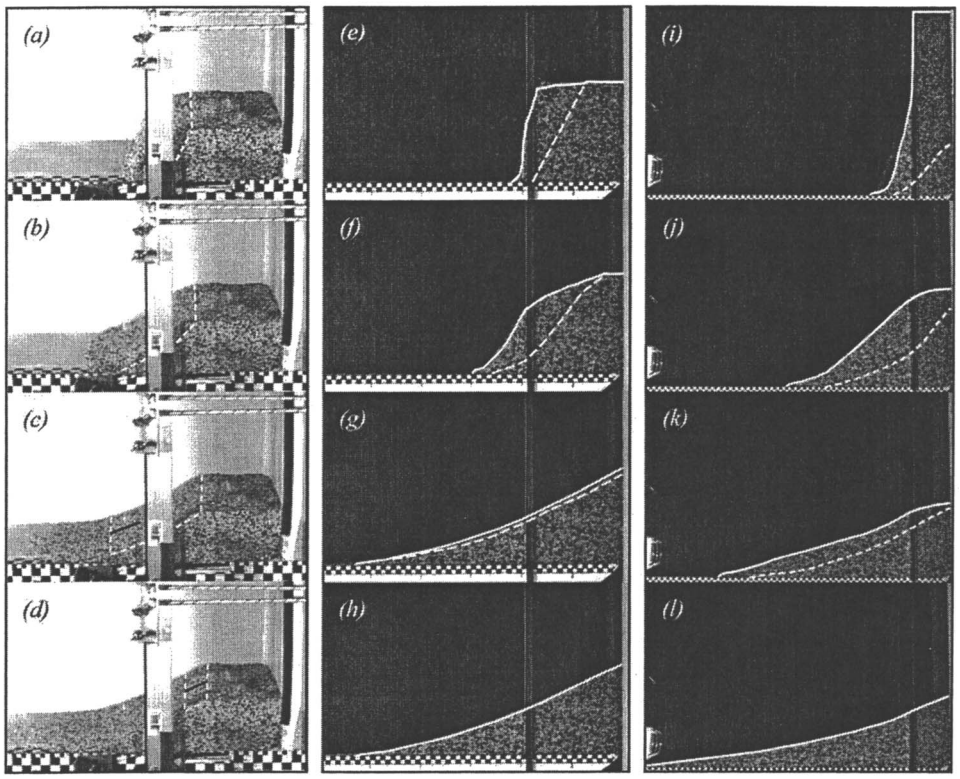

FIG. 3. Flow evolution at different times for experiments with $a=0.5$ (a)–(d), $a=1.5$ (e)–(h), and $a=7$ (i)–(l). The dashed curves mark the position of the interface between static and moving particles, whereas the solid curve highlights the upper free surface.

$$d_a/d_i = 0.99 - 0.54a. \quad (1)$$

This reveals that d_a becomes satisfyingly close to d_i as $a \to 0$. The difference between 0.99 and the expected value of 1 gives an indication of the magnitude of error in our experiments. The slope of 0.54 corresponds to an inclination to the horizontal of $\beta=61.6°$. Both these observations suggest that the inner, static body of material initially takes the form of a two-dimensional wedge with a corresponding aspect ratio of about 1.8.

For all aspect ratios, the flowing material passes through two characteristic phases of granular flow before the material arrests in its final configuration. In the first *spreading phase*, the flowing layer moves as a largely deforming, deep bulk flow. Particles originally at the free surface remain at the upper free surface or become incorporated into a thin basal layer when overrun by the flow front. In this phase of the collapse, the interface between moving and static grains propagates towards the upper free surface (Fig. 3) and continuously reduces the volume of the flowing layer. The flat frontal region quite abruptly ceases motion when the interface has reached the free surface and thereby determines the maximum runout at the end of the spreading phase. In analogy to our axisymmetric study, we define the time t_∞ as the duration of the spreading phase ending with the flow front coming to rest. At the steeper central slope, granular flow is observed to continue considerably longer than t_∞, in a phase that we refer to as the *final avalanching phase*. It consists of the backward propagation, along the free surface of the steep central slope, of the interface between already deposited and still moving grains [Figs. 3(c), 3(d), 3(g), and 3(h)]. The relatively slow granular motion takes the form of thin avalanches (a few grain diameters in depth) and modifies the free surface further. In Fig. 5 we show a plot of $(t_e - t_\infty)/t_e$ against the aspect ratio for fine and coarse sand, where t_e is the duration of the entire experiment. We observe that the nondimensionalized time of avalanching is a decreasing function of the aspect ratio for $a<4$ and remains rather constant (less than 0.2) for larger values of a. In addition, the duration of final avalanching strongly depends on the type of grain. This, as we will discuss later, is in contrast to t_∞, which appears to be independent of the grain type. For $a<1.8$, the final avalanches progressively erode the initially static part of the upper surface. Whereas for $a<1.15$ a static region on top of the initial column remains in the final deposit [Fig. 3(d)], the avalanches consume its entire area for $1.15<a<1.8$ [Fig. 3(h)]. For $a>1.8$, erosion by final avalanching appears to play a negligible role. Here the strongest alteration of the free surface by final avalanching at $x=0$

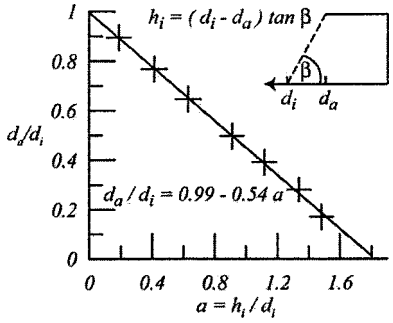

FIG. 4. The nondimensional horizontal distance of the undisturbed free surface, d_a/d_i, as a function of the aspect ratio from experiments of series A for $a<1.8$ with the best straight line fit through the data.

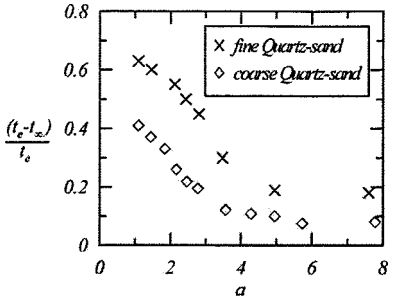

FIG. 5. The nondimensional duration of *final avalanching*, shown as the ratio $(t_e-t_\infty)/t_e$, as a function of the aspect ratio for fine and coarse quartz sand.

accounts to less than 2 mm for fine sand and not more than 1.5 mm for the other materials. Two major forms of final deposits can thus be distinguished: truncated wedges for $a<1.15$; and wedgelike deposits with a flatter frontal region and a steeper central region for a $a>1.15$. A third more or less flat form, as observed for the axisymmetric collapses [19], was not observed in the range of aspect ratios tested.

B. Internal deformation and sedimentation

Granular collapses within a channel allow the observation of internal deformation directly through the Plexiglas wall, which is an advantage to the previously studied axisymmetric experiments [19]. A major reason to conduct these experiments in a wide channel was to reduce the effects of frictional interaction with the walls which will certainly become important in the case of very narrow flumes. We analyzed the evolution of the velocity profiles at the free surface to constrain the influence of the walls on experimental results. Velocity profiles across the surface of the channels (Fig. 6) show contrasted features between the spreading and avalanching phases. The velocity profiles indicate plug flow for the spreading phase with minor shear at the walls and strong slip. The avalanching phase shows much stronger shear towards the walls and unsteadiness with simultaneous zones of no movement and actively flowing zones.

One way to illustrate the deformation of the flowing layer with time is to calculate the intensity differences between consecutive frames of a high-speed sequence. Typical results

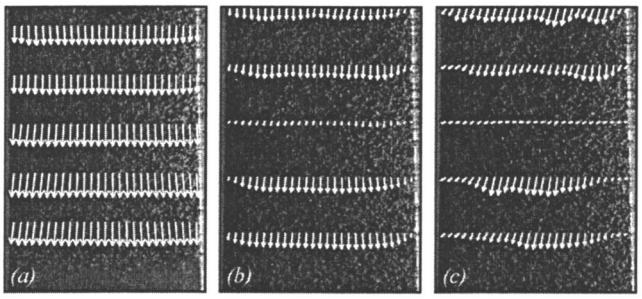

FIG. 6. Velocity profiles across the free surface during (a) the spreading phase, (b) the commencement, and (c) the end of the avalanching phase. To enhance visibility the length of velocity vectors are scaled by factors (a) of 2, (b) of 10, and (c) of 30.

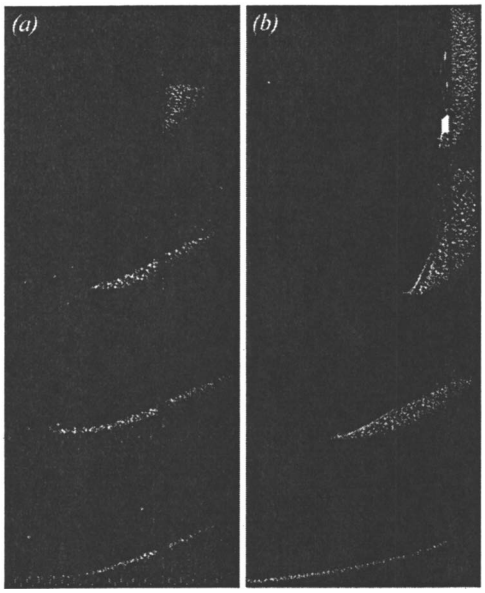

FIG. 7. Difference calculations between consecutive images of a high-speed sequence for (a) $a=1.5$ and (b) $a=5$ to visualize the evolution of the flowing layer with time.

of such calculations for low and high aspect ratio flows are shown in Fig. 7. Similar to axisymmetric collapses, only the frontal part of the flowing layer is in contact with the basal surface, whereas the major flow takes place over deposited material. In both flow regimes, the interface between moving and static particles first develops a strong concave upwards profile with the degree of concavity decreasing with time. Thus the lower and upper surfaces of the flowing layer become increasingly parallel until the two merge at the end of the spreading phase.

Velocity profiles with depth have been measured for large aspect ratio flows. Based on PIV measurements two transient stages of collapse become evident. The first stage is related to the constant acceleration of the flow front (see Sec. IV D), and the falling column can be divided into two zones of different behavior. The upper part of the column falls vertically as shown by the vertical vectors of similar length and the nondeforming top [Figs. 8(a) and 8(b)]. Deformation is restricted to the lower part of the column. Systematic measurements for different values of a indicate that the nondeforming upper part of the column develops above a height of about 2.8 d_i independent of h_i. Deformation of the top occurs when it becomes less than this critical height. Also, in this second stage of deformation, when the flow front moves at an approximately constant velocity, velocity profiles with depth are not linear and vary with the position in the flowing layer and time [Figs. 8(c) and 8(d)]. Figures 8(e)–8(g) show close-ups of the form of the velocity profile above the flowing/static interface with time. These may be subdivided into three transient vertical regions with an upper low-shear, pluglike zone, a middle region with an approximately linear gradient, and a lower exponential tail towards the interface. Velocity profiles in the frontal region with direct contact to the basal surface reveal a basal slip velocity and an approximately linear form above that.

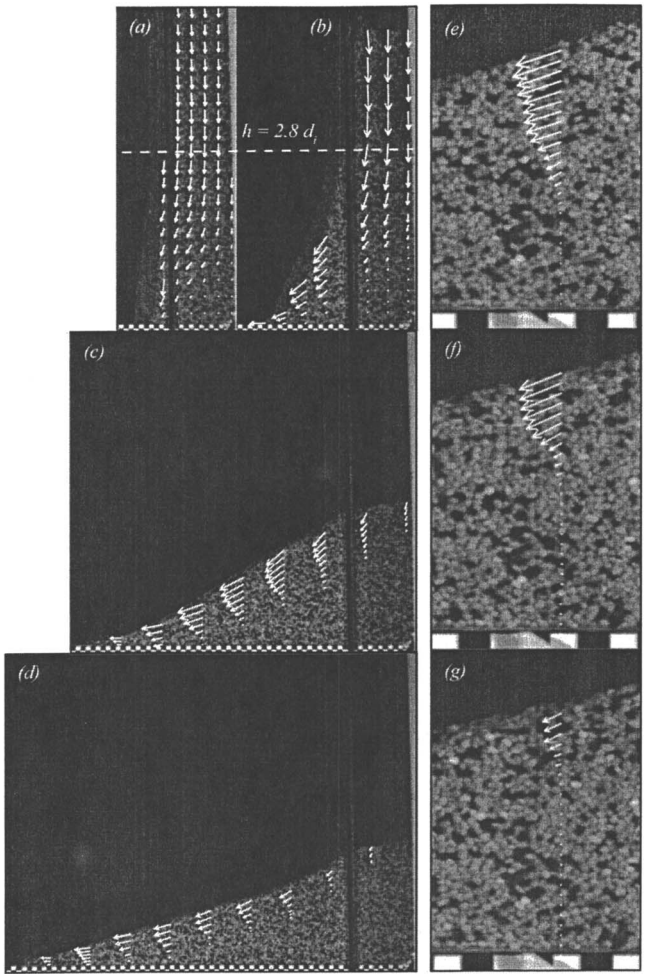

FIG. 8. Velocity profiles with depth at different times during the spreading phase for an experiment where $a=7$ (a)–(d), and close-ups of the evolution of the velocity profile with time for the same experiment at a distance $d_\infty/3$ (e)–(g).

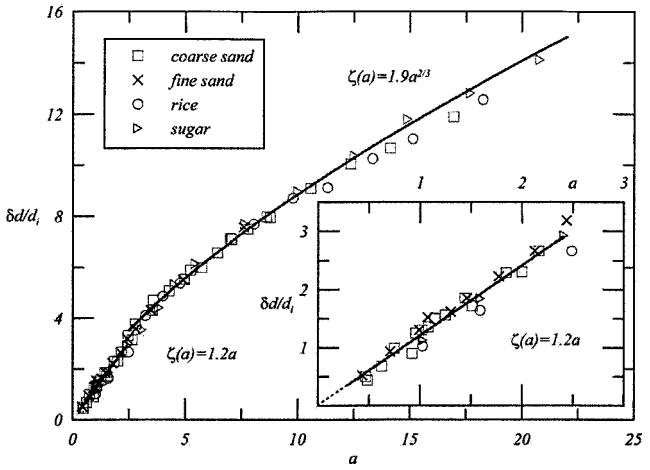

FIG. 9. The nondimensional incremental runout distance, $\delta d/d_i$, as a function of the aspect ratio for all our grains of series A. The inset highlights the data for small aspect ratios.

IV. QUANTITATIVE RESULTS

A. Scaling arguments for the final runout distance

Our observations that the form of collapses differ with different values of the aspect ratio $a=h_i/d_i$ immediately suggest using a as a fundamental parameter for the analysis of the final runout distances, d_∞. Arguments that a is the only parameter were presented in Lube *et al.* [19]. With the use of dimensional analysis we can then express d_∞ as

$$\delta d \equiv d_\infty - d_i = d_i \zeta(a), \tag{2}$$

where $\zeta(a)$ is a nondimensional function of the aspect ratio. In Fig. 9 we plot the incremental runout distance, δd, normalized by the initial basal length d_i, against the aspect ratio for all our different grains from series A. All the runout data collapses onto a single curve, suggesting that no further external parameters, such as the intergranular or basal friction, are needed for their mathematical description.

The function $\zeta(a)$ could theoretically take any form. However, for the low aspect ratio regime the function can be determined by simple physical arguments. Collapses for aspect ratios in this range display granular motion only beyond a specific distance d_a. The function $\zeta(a)$ must consequently be independent of the value of d_i. Thus in terms of Eq. (2) the initial height is the only length the incremental runout distance can be related to, and thus $\delta d=c_1 h_i$, and the functional form $\zeta(a)$ is given by

$$\zeta(a) = c_1 a \quad (a < 1.8). \tag{3}$$

The coefficient c_1 remains to be determined experimentally. For series A at low a the data are well represented by $\zeta(a)=1.2a$ (inset of Fig. 9).

For larger aspect ratios we cannot obtain a formulation for $\zeta(a)$ *a priori* by simple physical or dimensional arguments. A good representation of the experimental data, however, is given by the power-law form

$$\delta d/d_i = c_2 a^{2/3} \quad \text{with } c_2 = 1.9 \quad (a > 2.8). \tag{4}$$

Together with the analysis of the final height profiles, we give a geometrical explanation for this result in Sec. IV C. There is not an abrupt break in the curve $\zeta(a)$, but a small transitional region for $1.8<a<2.8$ exists between the linear and the power-law descriptions.

For the experiments of series B the same analysis can be applied. Again, the collapse of the data for three different values of d_i is obtained when the runout is plotted as a function of the aspect ratio (Fig. 10). Note that the data plotted in Fig. 10 include those taken from flows on sandpaper. The curve coincides in mathematical form with that given for experiments of series A with a linear section at low aspect ratios and a 2/3 power law for the large aspect ratio regime. The experimentally determined coefficients in Eqs. (3) and (4), however, are larger than those of series A with $c_1=1.6$ and $c_2=2.2$. Since all other experimental parameters are kept the same, these differences must reflect the different nature of collapse when the column supports itself during the experiment, as in series A, or flows between a static wall as in series B.

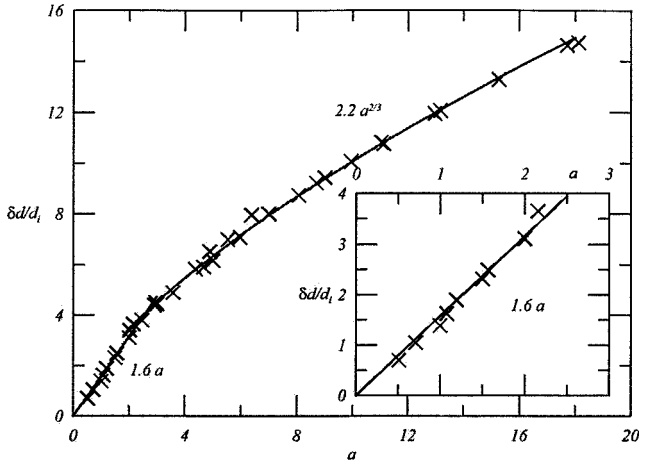

FIG. 10. The nondimensional incremental runout distance, $\delta d/d_i$, as a function of the aspect ratio for experiments of series B.

B. Scaling arguments for the maximum deposit height

The maximum deposit height at $x=0$ is dependent on the initial height and the aspect ratio and is a consequence of both the initial spreading phase and the late stage avalanching along the free surface. By dimensional analysis the final maximum height can be expressed as

$$h_\infty = d_i \varphi(a), \tag{5}$$

where $\varphi(a)$ is a nondimensional function of a. The function can be specified for small aspect ratio collapses where $h_\infty = h_i$ and thus

$$\varphi(a) = a, \tag{6}$$

as indicated by the data for $a \leqslant 1.15$ (Fig. 11). The expression for h_∞ is only linear, and independent of d_i, for $a \leqslant 1.15$, whereas the function for the maximum runout remains linear up to $a \sim 1.8$, the aspect ratio of static wedge. At $1.15 < a < 1.8$ an inner part of the upper surface of the column initially remains static but is then eroded by late stage avalanching.

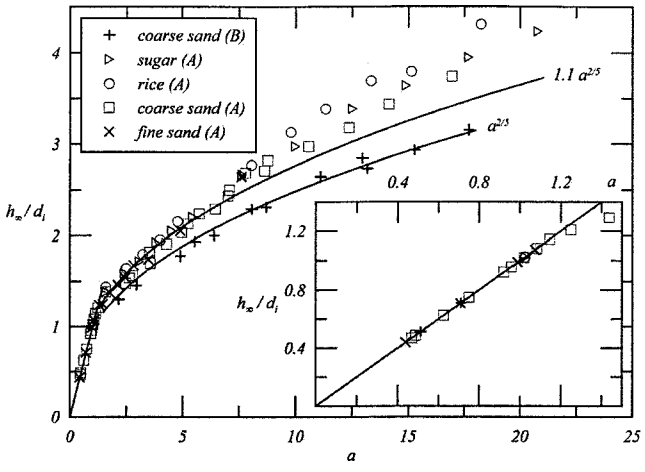

FIG. 11. The nondimensional maximum deposit height, h_∞/d_i, as a function of the aspect ratio. Functions of the form $\varphi(a) = ka^{2/5}$ are shown for experiments of series A and B. There is the tendency of series A data to increasingly deviate from the curve at large aspect ratios.

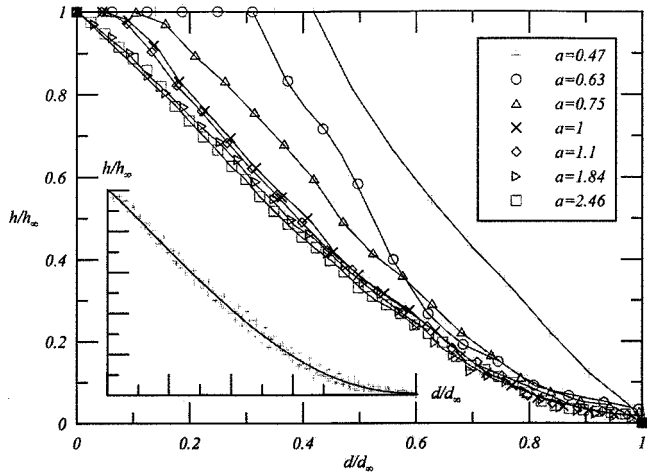

FIG. 12. The nondimensional height of the final deposits as a function of nondimensional distance for $a < 2.5$ for some series A experiments. The inset shows the same plot for $a > 2.8$.

For $a > 1.15$ the data suggest the functional form

$$\varphi(a) = ka^{2/5}, \tag{7}$$

with the constant k differing just slightly for experiments of series A ($k=1.1$) and B ($k=1$) (Fig. 11). Series A data further show a deviation from the functional form (7) for $a > 8$. We assume that this deviation is caused by frictional effects due to the vertical walls of the channel that become important during low-velocity grain motion during the final avalanche stage. This interpretation is supported by the fact that such a deviation is not observed for experiments in a wider channel (series B).

C. Final height profiles

The contour of the final deposits can be written in nondimensional form as

$$h(x)/h_\infty = \eta(x/d_\infty, a) \tag{8}$$

with η being a dimensionless function of x/d_∞ and a. In addition we know by definition that

$$\eta(0,a) = 1 \quad \text{and} \quad \eta(1,a) = 0. \tag{9}$$

The normalized final height profiles at low aspect ratios (Fig. 12) reveal the large variation of form with the aspect ratio. However, the normalization of our final height profile data for all large aspect ratio flows results in a collapse of all data points onto a universal curve (inset of Fig. 12). The minor scatter might be entirely explained by the modification of the deposit shape during the final avalanching stage. The important result from this analysis is that this normalized universal curve is independent of the value of the aspect ratio

$$h(x)/h_\infty = \eta(x/d_\infty) \quad (a > 2.8). \tag{10}$$

The integral of this curve gives A_n, defined by

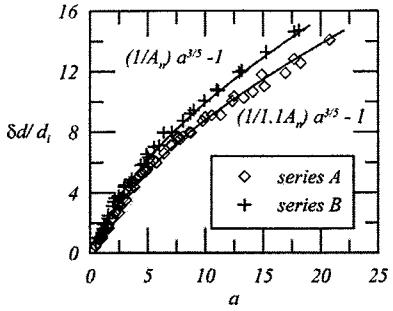

FIG. 13. The nondimensional incremental runout distance, $\delta d/d_i$, as a function of the aspect ratio for experiments of series A and B. The functions drawn through the data for the large a regime are of the form $\delta d/d_i = a^{3/5}/(A_n k) - 1$, where k is an experimentally determined coefficient from the analysis of h_∞ and A_n is the normalized cross-sectional area of the final deposits, calculated as $A_n \approx 0.37$.

$$A_n = \int_0^1 \eta(y)dy. \tag{11}$$

The integral was evaluated for series A and B data and gives nearly identical values for both curves with $A_n \approx 0.37$ (for $a > 2.8$).

We will use this result to discuss now the final runout data for large a. On a macroscopic scale, volume conservation must be valid for granular column collapses. For the two-dimensional spread we can thus assume that the initial and final cross-sectional areas in the flow direction are equal,

$$\int_0^{d_\infty} h(x)dx = h_\infty d_\infty \int_0^1 \eta(y)dy = h_i d_i. \tag{12}$$

Thus

$$\int_0^1 \eta(x)dx = \frac{h_i d_i}{h_\infty d_\infty}. \tag{13}$$

Substituting Eqs. (5) and (2), rewritten as $d_\infty = d_i f(a)$, into Eq. (12), we can write

$$\int_0^1 \eta(x)dx = a\frac{1}{\varphi(a)f(a)} \approx 0.37 \quad \text{(independent of } a\text{)}. \tag{14}$$

The expression (14) can only be independent of a if the product $\varphi(a)f(a)$ is directly proportional to a. We can use this relationship to calculate the final runout distance by using Eq. (7), the experimentally determined expression for h_∞, to determine that

$$d_\infty/d_i = a^{3/5}/(0.37k) \tag{15}$$

or

$$\delta d/d_i = a^{3/5}/(0.37k) - 1. \tag{16}$$

Using the experimentally determined coefficients k for series A and B we obtain a good fit to the runout data at $a > 2.8$ (Fig. 13). Although Eq. (16) reveals a geometrical relationship for the final runout distance at large aspect ratios a physical explanation remains a challenge for further studies.

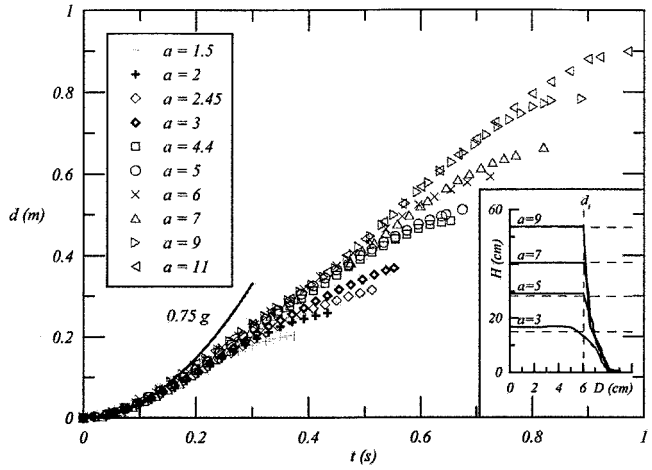

FIG. 14. The horizontal excursion of the flow front as a function of time for $d_i = 8.3$ cm. The inset compares profiles of the free surface for four experiments with $d_i = 6.05$ cm 83 ms after initial motion. Horizontal dashed lines mark the calculated free-fall heights of the top of the columns at this time.

D. Kinematic data

Data of the position of the flow front as a function of time were collected for aspect ratios in the range $0.5 < a < 18$ for different values of d_i. The typical form of the distance-time path is shown for $d_i = 8.3$ cm in Fig. 14. We clearly distinguish three transient stages, with an initial acceleration, a phase of approximately constant velocity and a final deceleration. The initial horizontal acceleration is constant at $0.75g$ for all values of d_i. The duration of constant velocity motion decreases with lower values of a and does not develop for $a < 1.5$.

From the high-speed movies we also determined the time, t_∞, at which the motion of the flow front ceases. By dimensional arguments it must be of the form

$$t_\infty = (d_i/g)^{1/2}\psi(a), \tag{17}$$

for some functional form of $\psi(a)$. For small values of the aspect ratio t_∞ must be independent of d_i and $\psi(a) = ca^{1/2}$. From Fig. 15 it is seen that the data for large aspect ratios are also well represented by $\psi(a) = 3.3a^{1/2}$, suggesting that the time for the columns to spread only depends on the value of h_i. Series A data shows a larger scatter around Eq. (17) which is due to the low frame rate of the charge coupled device footage from which it was measured. Note that a grain in free fall from height h_i would hit the ground in a time

$$t_0 = (2h_i/g)^{1/2} = (2ad_i/g)^{1/2} \approx 0.43t_\infty. \tag{18}$$

The initial collapse is driven by vertical free-fall behavior. This is confirmed by the experimental observation that the upper part of the column, above a height $\sim 2.8d_i$, undergoes undisturbed vertical motion. To further analyze this, we compared the free surface profiles of flows with aspect ratios 3, 5, 7, and 9 at a time 83 ms after initial motion (inset of Fig. 14). At this time the flow fronts for $a = 9$ and $a = 7$ still move

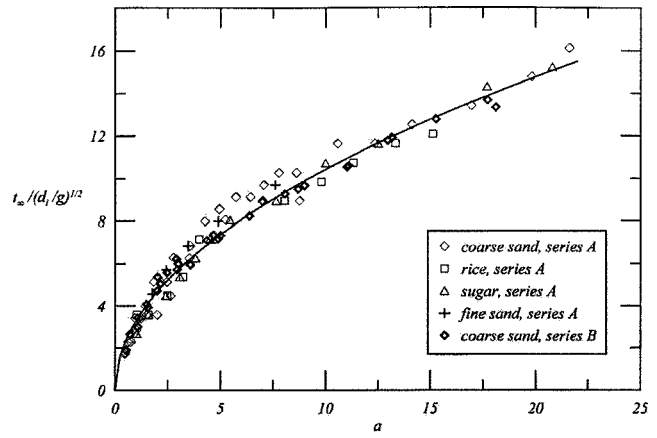

FIG. 15. The nondimensional time for the flow front to cease motion as a function of the aspect ratio with the curve $\psi(a)=3.3a^{1/2}$.

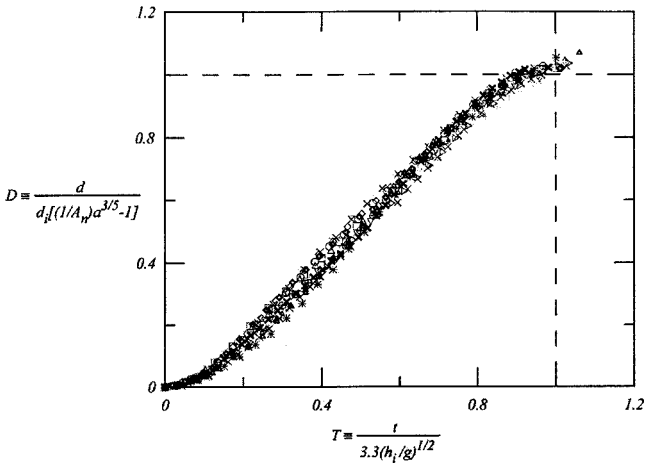

FIG. 16. The normalized distance-time data of the flow front for $a>2.8$ of series B.

at constant horizontal acceleration $0.75g$, while for $a=5$ the acceleration is smaller than $0.75g$, and for $a=3$ the motion of the flow front is already at constant velocity. The horizontal dashed lines correspond to the theoretical free-fall heights $h_f=h_i-0.5gt^2$ at $t=83$ ms. For $a=7$ and $a=9$ the tops of the columns match this relationship, but remain higher than h_f for $a=5$ and $a=3$. Hence the phase where the upper part of the column is in vertical free-fall corresponds to the stage of constant horizontal acceleration of the flow front. As long as the column height remains greater than $2.8d_i$ ($a\geqslant 5$ in Fig. 14) flow cross-sectional profiles remain self-similar as the flow front accelerates at $0.75g$. Lateral flowage during this stage is thus independent of h_i. The cross-sectional profile changes notably when the height falls below $2.8d_i$ ($a=3$ in Fig. 14) and the flow front assumes a constant velocity, indicating that the dominant control by the column's free-fall has terminated.

The distance and time data of flow front propagation can be expressed in nondimensional form as fractions of their terminal values (16), (17) such that

$$D \equiv d/d_\infty = d/[d_i(a^{3/5}/A_n) - 1] \tag{19}$$

and

$$T \equiv t/t_\infty = t/3.3(h_i/g)^{1/2}. \tag{20}$$

Figure 16 shows that this approach results in the collapse of all distance-time data onto a universal curve that preserves the three stages of initial acceleration, constant velocity, and terminal deceleration.

V. SUMMARY AND CONCLUSIONS

This paper presents detailed, quantitative observations of the collapse of a granular column in a two-dimensional manner down a horizontal channel. The experimental work complements two previous studies on axisymmetric granular column collapses on a horizontal base [19,20]. We carried out two different series of experiments: (A) symmetrical spreading, for which the two gates across the channel holding the column were lifted simultaneously and the column spread in a symmetrical manner up and down the channel; and (B) unidirectional spreading, for which only one retaining gate was lifted and the grains spread down the channel, constrained by the fixed backwall. The differences in flow behavior between these two situations were small. The main experimental results are as follows.

In each case there was a triangular wedge (or trapezoidal wedge for low aspect ratio columns) having the basal width of the column and making an angle of $61\pm2°$ with the horizontal, within which the grains never moved. Two forms of collapse were recorded, corresponding to a low aspect ratio regime, for $a<1.8$ ($=\tan 61°$), and a large aspect ratio regime, for $a>1.8$.

In both flow regimes the volume of flowing material reduced continuously by the propagation towards the upper free surface of the interface between static and flowing grains. The vertical velocity profiles between the interfaces varied both downstream and with time. The flow front propagated in a manner that varied with time. The flowing grains never contact the floor except for a small region just behind the flow front.

We distinguish two subsequent flow phases. In the initial spreading phase, most details of the final form of the deposit are established in time t_∞, independent of the type of grain, and effects of the limiting channel walls are minimal. The final avalanching phase includes the stabilization of the steep inner part of the pile via thin avalanches. Here strong velocity gradients across the free surface develop and the motion shows a clear temporal dependence on the grain type.

All data of the rescaled maximum horizontal and vertical excursion of the final deposit collapse onto single curves, as a function of the initial aspect ratio only, and independent of internal and basal friction. For low aspect ratios, these functions are linear, while they take a power-law form for high aspect ratios.

The time for collapse, t_∞, varies as the square root of the initial column height and is independent of its width. For $a>2.8$, the collapse is mainly controlled by the initial free-fall behavior of the column.

All collapses for $a>2.8$ generated self-similar deposit shapes that can be functionally described using volume con-

servation. As a consequence, nondimensional distance-time paths are also self-similar.

These results are not compatible with earlier continuum representations of granular flows that used the shallow water approximation and invoked roughly uniform vertical velocity profiles, small surface slopes, and heavily depend upon friction coefficients [6,10,13]. In our experiments the velocity profiles were not linear, the slopes were large, and friction was not important until the end. This last statement is in itself surprising and the explanation is that frictional effects are relatively small, just like a fluid flowing at high Reynolds number, until the velocity falls sufficiently that friction can dominate, and does so in this granular case quite rapidly. There is an interesting analogy, which can be pursued analytically, with a cooled and solidified liquid at low values of the Stefan number,

$$S = L/(c_p \Delta T), \tag{21}$$

where L is the latent heat, c_p the specific heat, and ΔT the temperature fall needed for the fluid to solidify. Latent heat effects are essential for the fluid to solidify, just as frictional effects are essential for the flow to cease. However, in the limit of low Stefan number, the time for solidification is independent of the explicit value of the latent heat. An alternative numerical approach would be to employ individual grain-following computations, which involve as many as 10^8 grains. However, these have generally produced results, which are heavily dependent upon intergranular friction and the exact shape of the grains [23–26]. Nevertheless, it might be interesting to pursue such an approach.

The results for two-dimensional collapses are all similar in spirit to those found for the axisymmetric case [19]. In both cases the dimensions of the final deposit and the collapse time are represented by similar functions, but the values of limiting aspect ratios and empirical constants differ.

We plan to present further insights regarding the dynamics of the interface between moving and deposited grains in subsequent papers.

Note added. We have recently become aware of two papers which appeared after the submission of our work. In [27] the authors detail the collapse of an essentially semi-infinite granular step of noncohesive steel beads ($a \sim 0$ in our notation) and propose a simple theoretical model which yields reasonable results, even though, in the authors' words "some of the assumptions in the model… are not met in the experiments." In [28] a shallow water model, based on small slopes of a spreading layer of grains, is presented. The agreement between the theoretical results and experiments by the author to be published in the future is not good. This is not surprising given that, as we explain herein, considerably less than half the time of the collapse is spent as a thin layer; and in that time the velocity profile is far from uniform, with much of the lower part of the layer stationary.

ACKNOWLEDGMENTS

G.L. and A.F. acknowledge support by the Deutsche Forschungsgemeinschaft. R.S.J.S. acknowledges a Royal Society—Wolfson merit award.

[1] H. M. Jaeger, S. R. Nagel, and R. P. Behringer, Rev. Mod. Phys. **68**, 1259 (1996).
[2] L. P. Kadanoff, Rev. Mod. Phys. **71**, 435 (1999).
[3] P. G. de Gennes, Rev. Mod. Phys. **71**, S374 (1999).
[4] G. B. Whitham, *Linear and Nonlinear Waves* (Wiley, New York, 1974).
[5] J. Pedlosky, *Geophysical Fluid Dynamics* (Springer-Verlag, New York, 1979).
[6] S. B. Savage and K. Hutter, J. Fluid Mech. **199**, 177 (1989).
[7] K. G. Anderson and R. Jackson, J. Fluid Mech. **92**, 145 (1992).
[8] S. B. Savage, J. Fluid Mech. **377**, 1 (1998).
[9] O. Pouliquen and Y. O. Forterre, J. Fluid Mech. **453**, 133 (2002).
[10] R. M. Iverson and R. P. Denlinger, J. Geophys. Res. **106**, 537 (2001).
[11] K. J. Hsü, Geol. Soc. Am. Bull. **86**, 129 (1975).
[12] B. Voigt, *Rockslides and Avalanches*, *Vol. 1* (Elsevier, New York, 1978).
[13] K. Hutter, T. Koch, C. Plüss, and S. B. Savage, Acta Mech. **109**, 127 (1995).
[14] R. M. Iverson, Rev. Geophys. **35**, 245 (1997).
[15] H. E. Huppert and W. B. Dade, Theor. Comput. Fluid Dyn. **10**, 201 (1998).
[16] W. B. Dade and H. E. Huppert, Geology **26**, 803 (1998).
[17] GDR MIDI, Eur. Phys. J. E **14**, 341 (2004).
[18] P. Jop, Y. Forterre, and O. Pouliquen, J. Fluid Mech. **541**, 167 (2005).
[19] G. Lube, H. E. Huppert, R. S. J. Sparks, and M. A. Hallworth, J. Fluid Mech. **508**, 175 (2004).
[20] E. Lajeunesse, A. Mangeney-Castelnau, and J. P. Vilotte, Phys. Fluids **16**, 2371 (2004).
[21] H. E. Huppert, M. A. Hallworth, G. Lube, and R. S. J. Sparks, Bull. Am. Phys. Soc. **48**, 68 (2003).
[22] S. B. Dalziel, *DigiFlow User Guide*, http://www.damtp.cam.ac.uk/lab/digiflow/ (2005).
[23] G. S. Campbell, Annu. Rev. Fluid Mech. **22**, 57 (1990).
[24] T. Shinbrot, A. Alexander, M. Moakher, and F. J. Muzzio, Chaos **9**, 611 (1999).
[25] P. W. Cleary and M. L. Sawley, in*Proceedings of the 2nd International Conference on CFD in the Minerals and Process Industries*, CSIRO, Melbourne, Australia (1999).
[26] R. Zenit, Phys. Fluids **17**, 031703 (2005).
[27] S. Siavoshi and A. Kudrolli, Phys. Rev. E **71**, 051302 (2005).
[28] R. R. Kerswell, Phys. Fluids **17**, 057101 (2005).